# Binding of ncd to Microtubules Induces a Conformational Change near the Junction of the Motor Domain with the Neck†

Nariman Naber,*,‡ Roger Cooke,‡ and Edward Pate§

*Department of Biochemistry and Biophysics and Cardiovascular Research Institute, University of California, San Francisco, California 94143, and Department of Pure and Applied Mathematics, Washington State University, Pullman, Washington 99164*

*Received March 25, 1997; Revised Manuscript Received May 9, 1997*⊗

ABSTRACT: We have covalently attached an electron paramagnetic resonance (EPR) spin probe to Cys-670 of the motor domain of ncd (nonclaret disjunctional protein) in order to investigate conformational changes associated with the chemomechanical cycle. Spin-labeling is highly specific and does not affect ncd function as monitored by either the binding affinity to microtubules or the rate of ATP hydrolysis. The EPR spectra can be deconvoluted into two components, one that is highly mobile with respect to the protein and one that is strongly immobilized. In the absence of microtubules, the relative proportions of these two components varied with temperature, showing that the transition between them involves a large change in enthalpy ($\Delta H° = -75$ kJ/mol). This result implies that the two populations represent very different protein conformations. Binding to microtubules results in virtually all probes shifting into the immobilized component, independent of the nucleotide bound. Superposition of the structures of ncd and myosin subfragment 1 reveals that the labeled cysteine is very close to the region which is homologous to the helix containing the two reactive sulfhydryls in myosin and is ∼10 Å from the junction of the motor domain with the remainder of the molecule. We conclude that the binding of ncd to microtubules results in a conformational change in this region which may be involved in the working power stroke.

Nonclaret disjunctional protein (ncd)[1] is a motor protein of the kinesin family which cyclically interacts with microtubules via hydrolysis of MgATP to translocate organelles within the cytosol. A fundamental and as yet unresolved question in cell motility is to identify the conformational changes within both microtubule- and actin-based motor proteins during their working cycle. The recent X-ray crystallographic structures of the motor domains of kinesin and ncd (*1, 2*), and the actin-based motor myosin (*3*−*5*), have brought new potential for answering this question. For the first time, interpretation of experimental data is now both aided and constrained by the known location of individual amino acid residues in the motor proteins themselves. Additionally, there are obvious topological similarities in primary and secondary structure between the motor domain crystal structures of kinesin, ncd, and myosin, suggesting the likelihood that a common, fundamental motor mechanism may exist (*1, 2, 6*). Thus any insights into the working of one motor has the additional advantage of providing potential insights into the working of the other motors.

Historically, myosin has been a more extensively employed model system for motility studies than the more recently discovered ncd and kinesin motors. One frequently employed approach to investigate conformational changes in myosin has been through the use of electron paramagnetic resonance (EPR) probes. These have been either covalently attached to myosin (*7*−*9*) or introduced into the contractile system via paramagnetic moieties attached to substrate analogs (*10, 11*). Here we report the extension of EPR protocols to the study of ncd. We have covalently attached a maleimide EPR probe to a bacterially expressed motor domain (Arg-335−Lys-700) of *Drosophila* ncd at Cys-670. This construct contains a single, monomeric motor domain along with a short region which would lie between the motor domain and the coiled-coiled tail region. The reactive sulfhydryl in ncd identified here lies in the region of ncd that forms the junction between the head and the coiled-coiled tail of the molecule. By coincidence, the cysteine is located either in, or adjacent to, an α-helix that is structurally homologous to the helix in myosin that contains the reactive sulfhydryls, Cys-697, and Cys-707. Modifications of myosin at these reactive sulfhydryls result in a significant down-regulation of motor function (*12*, *13*). In stark contrast, however, we found that reaction of Cys-670 with the spin-label caused no impairment of ncd function. The EPR spectra indicated that this region of the molecule exists in two conformations for ncd free in solution and that one of these conformations is greatly favored by binding to microtubules.

## METHODS

*Protein Preparation. Drosophila* ncd motor domain (amino acids 335−700) was expressed in *Escherichia coli*, harvested, and stored until ready for use as described in

† These studies have been supported by USPHS Grants AR39643 (E.P.) and AR42895 (R.C.).

* Corresponding author. Tel: 415-476-1975, 415-502-6143. Fax: 415-476-1902. E-mail: NABER@NIIHAU.UCSF.EDU.

‡ University of California.

§ Washington State University.

⊗ Abstract published in *Advance ACS Abstracts,* July 1, 1997.

[1] Abbreviations: AMPPNP, adenosine 5′-(β,γ-imido)triphosphate; EGTA, ethylene glycol bis(β-aminoethyl ether)-*N*,*N*,*N*′,*N*′-tetraacetic acid; MSL, 4-maleimido-2,2,6,6-tetramethyl-1-piperidinyloxy; EPR, electron paramagnetic resonance; ncd, nonclaret disjunctional protein; MT, microtubules; PIPES, piperazine-*N*,*N*′-bis(2-ethanesulfonic acid); SL-ncd, construct consisting of the C-terminal 336 amino acids of *Drosophila* ncd with MSL covalently attached at Cys-670; TFA, trifluoroacetic acid; TPCK, L-1-(tosylamino)-2-phenylethyl chloromethyl ketone.

S0006-2960(97)00688-0 CCC: $14.00 

Shimuzu et al. (*14*). The construct is a monomer in solution. For spin-labeling of ncd, the protein was exchanged on a size exclusion column into a buffer containing 0.1 M NaCl, 1 mM EGTA, 2 mM $MgCl_2$, 20 mM PIPES, and 0.2 mM $Na_2ATP$, pH 7.0, 0 °C (buffer A). The protein concentration was ~ 50 $\mu$M. A 2-fold molar excess of MSL over ncd was added, and except as noted, the reaction allowed to proceed on ice for 1 h. Unreacted MSL was removed by again passing the protein over a size exclusion column and eluting with buffer A. The protein was then concentrated by centrifugation through a semipermeable membrane (Centricon, 30 kDa cutoff) with an excess of ATP over ncd monomer in the final protein sample. All spin-labeled ncd (SL-ncd) was used within 8 h of the labeling step. Protein concentrations were determined by the method of Bradford (*15*). The molecular mass of ncd was taken to be 41 kDa.

Tubulin was prepared from bovine brain tissue via repeated polymerization−depolymerization steps (*16*) following the protocols of Ma and Taylor (*17*). Tubulin was stored in a buffer containing 0.1 M PIPES, 1 mM EGTA, 1 mM $MgCl_2$, and 1 mM $Na_2GTP$, pH 6.9, −80 °C, until used. Microtubules were prepared immediately prior to use as follows. The tubulin was thawed and spun at 100000*g* for 20 min, 4 °C, to remove any aggregated tubulin. The supernatant was collected, and 1 mM $Na_2GTP$, 20 $\mu$M taxol, and 2 mM $MgCl_2$ were added. The mixture was then heated at 37 °C for 30 min to induce polymerization. The microtubules were spun down at 100000*g* for 25 min, the supernatant was discarded, and except as noted below, the microtubule pellet was resuspended in a buffer containing 25 mM PIPES, 2 mM $MgCl_2$, 20 $\mu$M taxol, 1 mM EGTA, 0.1 M NaCl, and 0.1% $NaN_3$, pH 7, 25 °C, at a concentration of 150−200 $\mu$M. All microtubules were used within 10 h of the polymerization step. The molecular mass of the $\alpha\beta$-tubulin dimer was taken to be 110 kDa.

*EPR Spectroscopy.* EPR measurements were performed with an ER/200D EPR spectrometer from IBM Instruments, Inc. (Danbury, CT). First derivative, X-band spectra were recorded using 50 s, 100 mT wide sweeps with the following instrument settings: microwave power, 25 mW; gain, $(0.1-1.0) \times 10^6$; center field, 3478−3480 mT; time constant, 200 ms; frequency, 9.3 GHz; modulation, 1 mT at a frequency of 100 kHz. Each spectrum used in data analysis represents the average of 5−25 distinct sweeps from an individual experimental preparation. Mixtures of microtubules and SL-ncd were mounted in a 50 $\mu$L glass capillary and placed in the center of a $TE_{011}$ cavity. The microtubule−SL-ncd pellets resulting from centrifugation were instead mounted on a rexolite flat cell, surrounded by grease, covered with a glass coverslip to prevent dehydration, and then placed in the cavity. Most EPR experiments were done at room temperature, 21−23 °C. For some experiments, temperature was controlled by blowing air (warm or cool) into the cavity and monitoring temperature via a thermistor placed close to the experimental sample. For experiments involving added ADP (AMPPNP), 2 mM $Na_2ADP$ ($Li_4AMPPNP$) and 5 mM $MgCl_2$ were added to the experimental buffer. For experiments involving AMPPNP, 0.1 mg/mL apyrase was also added to remove any ADP or ATP contamination present in commercially obtained AMPPNP (*18*). Apyrase-containing buffers were allowed to sit at room temperature for 45 min prior to use. To determine the low-field to high-field splitting in the rigid limit, SL-ncd was precipitated using ammonium sulfate and centrifuged. The pellet was mounted on the flat cell as described above.

For experiments involving ATP, buffer A was modified to contain 34 mM phosphocreatine, in lieu of 0.1 M NaCl, maintaining constant ionic strength, and the $Na_2ATP$ concentration was raised to 2 mM. Immediately prior to data collection, 1 mg/mL creatine phosphokinase was added in order to buffer ADP concentrations produced by the SL-ncd ATPase. For experiments in the absence of microtubules, SL-ncd was allowed to sit in the ATP-containing buffer for 10 min prior to data collection. In order to minimize changes in ionic strength due to the microtubule-activated, SL-ncd ATPase rate (affecting both the ATPase rate and the affinity of ncd for microtubules), EPR data collection in the presence of microtubules was terminated when a calculated 10% of the phosphocreatine had been used to convert ADP to ATP in the creatine phosphokinase catalyzed reaction. This limited our resolution to the average of five spectral sweeps. The stability of microtubule-based motor proteins decreases in the absence of bound nucleotide (*14*, *19*). Thus no experiments were attempted under "rigor" conditions. $Na_2ATP$, creatine phosphokinase, phosphocreatine, apyrase (type V), and $Li_4AMPPNP$ were obtained from Sigma Chemical Co. Taxol was obtained from Molecular Probes. TPCK-treated trypsin was purchased from Worthington Biochemical Corp.

*Peptide Separation and Sequencing.* The ncd construct employed in these experiments contains six cysteines. To determine which cysteine was being spin-labeled by MSL, the protein was cleaved proteolytically and the peptides were separated by HPLC using a modification of the protocols of Kanaani et al. (*20*). SL-ncd (approximately 3 mg/mL) was dialyzed overnight against 80 mM $NH_4HCO_3$, pH 7.8. The solution was briefly centrifuged to remove any precipitated protein, and the protein concentration was adjusted to 1 mg/mL by addition of a solution containing 80 mM $NH_4HCO_3$, pH 7.8. Urea was added as a solid until saturation was achieved (~8 M), and the mixture was incubated at 37 °C for 30 min. The buffer was then adjusted to 2 M urea with 80 mM $NH_4HCO_3$, pH 7.8, and 0.05 mg/mL TPCK-treated trypsin was added. TPCK-treated trypsin was from a 1 mg/mL stock solution in 0.1 N HCl which was stored at −80 °C until ready for use. Digestion proceeded at room temperature for 6 h. Another 0.05 mg/mL trypsin was added, and the digestion was allowed to continue overnight at room temperature. The trypsin-digested protein (250 $\mu$g) was separated by reverse-phase HPLC on a Rainin Microsorb-MV C-18 300 Å column (5 mm, 4.6 × 250 mm). Separation was accomplished with a linear gradient of 0.1% TFA in water (buffer B) and 95% acetonitrile in water containing 0.08% TFA (buffer C). Fractions of 1 mL were collected at a flow rate of 1 mL/min using a Rainin HPLX gradient HPLC system and a Dynamax UV-1 absorbance detector operating at 214 nm. The fractions were checked for the presence of spin probe using EPR spectroscopy. Detectable electron paramagnetism was present in only one fraction. Amino acid sequencing of the remainder of this fraction was done by Edman degradation in the Biomolecular Resource Center, UCSF.

*ATPase Activities and Binding Affinities.* SL-ncd ATPase activities were determined in buffer A, modified to contain 20 $\mu$M SL-ncd and 2 mM $Na_2ATP$, 25 °C. Control experiments used 20 $\mu$M unmodified ncd which went through

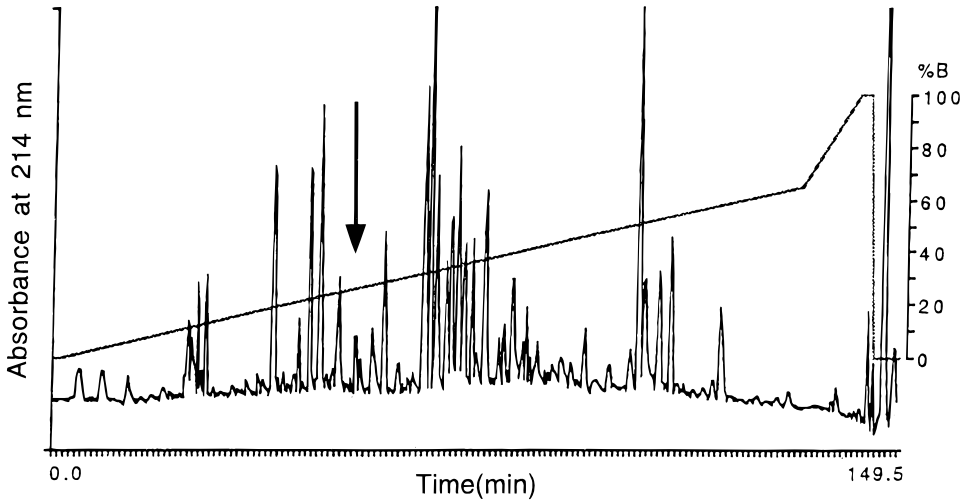


FIGURE 1: Reverse-phase HPLC separation of the tryptic digestion of SL-ncd. The linear gradient went from 0% to 65% buffer C (Methods) in 130 min, and then 65% buffer C to 100% buffer C in 10 min at a flow rate of 1 mL/min. The protein was detected at 214 nm. The fraction which eluted at 55 min, noted by the arrow, contained MSL-labeled Cys-670.

all handling steps of SL-ncd with the sole exception of omitting MSL from the actual labeling step. Liberated phosphate was determined every 30 min over a 2 h time period using the malachite green assay (*21*). A least-squares linear fit to the accumulated data gave the ATPase rate. For determination of the microtubule-activated ATPase, the ncd concentration was reduced to 2 $\mu$M, and the ATPase assay was initiated by addition of 20 $\mu$M microtubules. (For notational convenience, here and elsewhere, we shall refer to the concentration of "microtubules" to mean the polymerized $\alpha\beta$-tubulin dimer content.) Liberated phosphate was determined every 60 s over a 300 s time period.

Dissociation constants of ncd and SL-ncd from microtubules in the presence of either ADP or AMPPNP were determined using 2 mM ADP or AMPPNP, 35−50 $\mu$M unlabeled ncd or SL-ncd, and 45−75 $\mu$M microtubules in buffer A, 25 °C. The dissociation constant in the presence of 2 mM ATP was determined using the previously discussed modifications to buffer A. For binding studies, unlabeled ncd was again subjected to all handling steps used for SL-ncd, except omitting the addition of MSL. For experiments involving AMPPNP, 0.1 mg/mL apyrase was also added and the reaction mixture allowed to sit at room temperature for 45 min prior to use. The experimental mixture was centrifuged at 100000*g* for 25 min. The protein remaining in the supernatant was assayed using the method of Bradford (*15*) and a binding constant determined assuming that all protein in the supernatant was ncd. Control experiments using microtubules with no added ncd indicated that <0.2% of the microtubular protein remained in solution following centrifugation. Dissociation constants for SL-ncd from microtubules were also determined using the residual EPR spectra of the supernatant as discussed further in Results.

Data are given as mean ± SEM (numbers of observations), except in Figure 3 where the standard deviation is used.

## RESULTS

*Spin-Label Location.* Figure 1 shows the reverse-phase HPLC separation of the tryptic digestion of SL-ncd. All 150 fractions were individually checked for the presence of an EPR signal. Only the single fraction eluting at 55 min provided a detectable spin (noted with an arrow). Edman degradation sequencing showed the fraction to be a single peptide and gave the first five amino acids in the sequence to be F-A-A-S-V. Comparison of this fragment with the amino acid (aa) sequence of the ncd construct showed these could only be aa 663−667. The absence of an intervening tryptic cleavage site identified Cys-670 as the location of the spin-label.

*Specificity and Extent of the Spin-Labeling of ncd.* In the process of scanning the tryptic digestion fragments for the presence of electron paramagnetism, an EPR signal intensity equal to 5% of that obtained from the Cys-670 protein fraction would have been readily detectable. Using this as a conservative limit for our sensitivity and assuming that the other five cysteines in the ncd construct all had equal probability of reacting with MSL, we conclude that ≥80% of the covalently attached MSL was at Cys-670. It has generally been observed that cysteines in proteins can vary significantly in their reactivity (viz. the reactivity of SH-1 and SH-2 vs the other cysteines in myosin). In the case of the ncd construct employed in these studies, the X-ray crystallographic structure (*2*) indicated that two of the ncd cysteines (Cys-353 and Cys-429) were buried deep within the interior of the protein and that the side chain of one closer to the surface (Cys-368) pointed into the interior of the protein. Hence, a significant fraction of the six ncd cysteines (at least half) probably reacted poorly, if at all. Thus, our conclusion that ≤20% of the total labeling was at sites other than Cys-670 represents a fairly conservative estimate.

Additional arguments supported our conclusion that Cys-670 was our primary labeling site. The fraction of ncd molecules which were MSL-labeled was determined by quantitative EPR spectroscopy. Denaturation of the protein with 8 M urea produced a sharper EPR signal which could be more easily quantitated. A comparison of the double integral of this spectrum with that of a standard showed that the ratio of bound MSL to total protein was 0.94 ± 0.07 (six distinct labeling efforts). Neither variation of the time ncd was reacted with the label (15 min−24 h) nor doubling the ratio of spin label to protein in the reaction mixture altered the stoichiometry of the covalently attached spin label, strengthening the conclusion that we were labeling only a single, hyperreactive cysteine (i.e., Cys-670).

Table 1: Biochemical Parameters Used To Assess the Effect of MSL Labeling of ncd[a]

| observation | ncd | SL-ncd |
|---|---|---|
| ATPase ($s^{-1}$ per ncd) | $0.0038 \pm 0.0006$ (4) | $0.0082 \pm 0.0003$ (4) |
| microtubule-activated ATPase ($s^{-1}$ per ncd) | $0.29 \pm 0.01$ (3) | $0.33 \pm 0.02$ (3) |
| microtubule $K_d$ ($\mu$M), 2 mM ADP, protein assay | $26.6 \pm 4.6$ (4) | $44.7 \pm 3.3$ (4) |
| microtubule $K_d$ ($\mu$M), 2 mM ADP, EPR | nd | $49.5 \pm 3.5$ (5) |
| microtubule $K_d$ ($\mu$M), 2 mM AMPPNP, protein assay | $12.9 \pm 1.7$ (3) | $8.5 \pm 0.4$ (3) |
| microtubule $K_d$ ($\mu$M), 2 mM AMPPNP, EPR | nd | $5.8 \pm 1.2$ (5) |
| microtubule $K_d$ ($\mu$M), 2 mM ATP, EPR | nd | $61.7 \pm 1.4$ (6) |

[a] Protein assay refers to measurements of the microtubule dissociation constant, $K_d$, via determination of the residual solution protein by the method of Bradford (*15*) following centrifugation. EPR refers to determination of $K_d$ via the determination of solution protein by using the residual, solution EPR signal following centrifugation. nd = not determined.

*Effects of Spin-Labeling on ncd Function.* Table 1 gives the rate of ATP hydrolysis for ncd and SL-ncd in the absence and presence of microtubules. As is evident, labeled and unlabeled protein gave similar values for the ATPase activities. The ATPase values we obtained were in the range previously suggested by Shimizu et al. (*14*) at the 140 mM ionic strength used in our studies. Table 1 also gives dissociation constants for ncd and SL-ncd from microtubules in the presence of 2 mM ADP or AMPPNP as determined from sedimentation assays. As is evident, spin-labeling of ncd did not significantly affect binding. The dissociation constants were a factor of 5−10 less than observed for ncd at 40 mM ionic strength (*14*). However, for both ncd (*14*) and the related motor protein, kinesin (*17*), comparable decreases in the binding affinity have been observed when the ionic strength was raised to >100 mM. The binding affinity for SL-ncd was also assayed using EPR spectroscopy as discussed below.

*EPR Spectra.* The solid line in Figure 2a shows the EPR spectrum obtained from 50 $\mu$M SL-ncd in the presence of 2 mM ADP but in the absence of microtubules. No significant difference in the spectra for SL-ncd·ligand free in solution was observed when 2 mM AMPPNP or 2 mM ATP was substituted for the ADP of Figure 2a (Discussion). Addition of 50 $\mu$M microtubules to SL-ncd·ADP resulted in a fraction of the SL-ncd being in a bound, SL-ncd·ADP·MT state and caused a shift in the spectrum toward that of a more immobilized probe (Figure 2b). These modifications were most easily observed via the changes at the locations noted by arrows $P_1$, $P_2$, and $P_3$ in Figure 2. The spectral peak denoted by arrow $P_2$ arises from MSL spin probes which are covalently attached to Cys-670 of SL-ncd but are very mobile with respect to the protein (see Discussion). In the EPR spectra obtained from SL-ncd in solution in the presence of microtubules, there is a clear increase in the spectral intensity at the low-field peak, $P_1$, and the high-field dip, $P_3$, showing that the binding of SL-ncd to microtubules favors a more immobile spin probe.

In the presence of 2 mM AMPPNP or ATP, addition of microtubules caused a similar shift toward a more immobilized probe spectrum, but to varying degrees. In order to better correlate the observed spectral changes with the fraction of motors in the SL-ncd·ligand·MT state, some microtubule−SL-ncd buffer mixtures were centrifuged at 100000*g* for 25 min, pelleting the microtubules and bound SL-ncd·ligand. The supernatant was assayed via EPR spectroscopy, and the residual SL-ncd·ligand concentration was determined by comparison of the signal intensity with that obtained from a known SL-ncd·ligand concentration (e.g., Figure 2a). A dissociation constant was calculated,

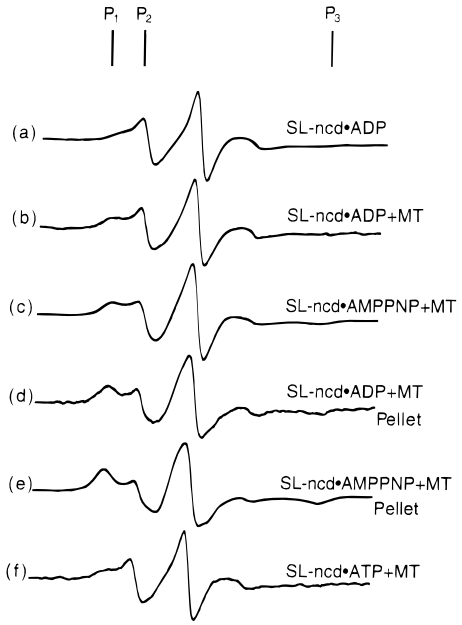


FIGURE 2: EPR spectra obtained from SL-ncd in the presence of varying ligands and in the presence and absence of microtubules. All experiments were done in buffers containing 50 $\mu$M SL-ncd, with the exception of (f) where the SL-ncd concentration was 35 $\mu$M. The polymerized tubulin concentration was 50 $\mu$M for all spectra involving the presence of microtubules. The ligand concentration was 2 mM in all cases. (a) EPR spectrum of SL-ncd·ADP free in solution. No statistically significant difference was observed when AMPPNP or ATP was the solution ligand. (b) EPR spectrum of SL-ncd·ADP·MT (MT = microtubules) free in solution. (c) EPR spectrum obtained from the sedimentation pellet of (b). (d, e) As with (b, c) except that AMPPNP was the ligand. (f) As with (b) except that ATP was the ligand.

with values given in Table 1. As is evident, the values obtained using EPR spectroscopy to monitor residual solution protein for a given set of experimental conditions were very similar to those obtained when the residual solution was assayed using the method of Bradford (*15*). Thus the presence of the spin probe itself is not influencing the binding assays.

The proportion of SL-ncd in bound, SL-ncd·ligand·MT states was enhanced in the microtubule−SL-ncd pellets. Figure 2d,e shows the enhancement of the immobilized component of the spectra (arrows $P_1$ and $P_3$) at the expense of the mobile peak (arrow $P_2$) using pellets obtained in the presence of ADP and AMPPNP. As shown in the Discussion, the magnitudes of the spectral shifts depended directly on the fraction of SL-ncd bound under the different conditions. No pellet was possible in experiments involving ATP, SL-ncd, and microtubules since we could not buffer ATP concentrations in the pellet.

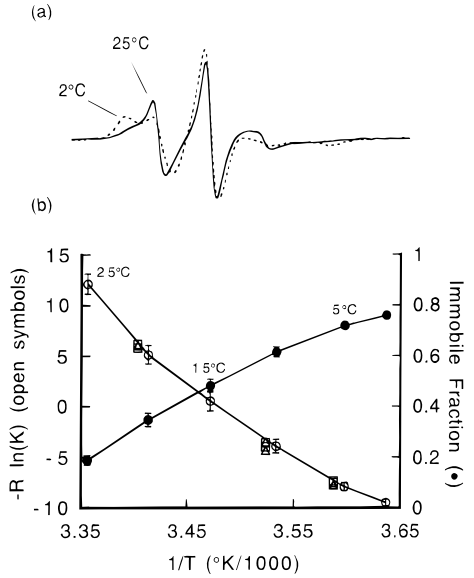


FIGURE 3: Temperature dependence of the immobilized fraction of probes on SL-ncd. (a) Spectra obtained from 50 $\mu$M SL-ncd in solution at 2 °C (solid line) and 25 °C (dashed line). (b) Right vertical axis: immobilized fraction as a function of 1/temperature for SL-ncd·ADP. Left vertical axis: $-R$ ln($K$) as a function of 1/temperature; $K$ = [immobile fraction]/[mobile fraction]. Open circles, triangles, and squares are with ADP, AMPPNP, and ATP as ligand, respectively. The ADP data are given as the mean ± SD from four to six observations. The less extensive data for AMPPNP and ATP (5, 10, 20 °C) are offset by 0.01 unit on the horizontal axis for better display and are within the experimental scatter of the ADP data.

Additional experiments investigated the effects of temperature on the EPR spectra of SL-ncd·nucleotide in solution. Figure 3a shows spectra obtained with ADP as the ligand at 2 °C (dashed line) and 25 °C (solid line). As is evident, there is a shift from the mobile, $P_2$, component to the immobile, $P_1$, component as the temperature decreases. As shown in the Discussion and Figure 3b, these data can be used to define the thermodynamics of the immobile-to-mobile transition.

## DISCUSSION

*Location of ncd Cys-670: Comparison with Myosin.* The recent X-ray crystallographic structures of several monomeric motor protein domains, along with electron cryomicroscopy based three-dimensional reconstructions of dimeric forms, allow our results to be put in better perspective. Figure 4 shows an overlay of the crystallographic structures of the ncd motor domain (*2*) and chicken myosin S1 (*3*). The structures in Figure 4 were aligned via simultaneous, least-squares distance superposition of both the Walker A (*22*), "P-loop" sequences (conserved amino acid sequence $Gx_4$-GKT in the motor proteins, aa 434−442 in ncd, aa 179−186 in chicken myosin) and the switch II regions (conserved amino acid sequence DxxGxE in the motor proteins, aa 580−585 in ncd, aa 463−468 in chicken myosin), both of which are adjacent to the nucleotide binding sites. As has previously been noted, when the structures of ncd, kinesin, and myosin S1 are aligned, selected secondary structural elements are seen to coincide (*1, 2*).

To facilitate discussion, we start with the structure of S1. The broken α-helix displayed as a ribbon diagram in the S1 structure of Figure 4 (colored dark blue; aa 689−710) is the

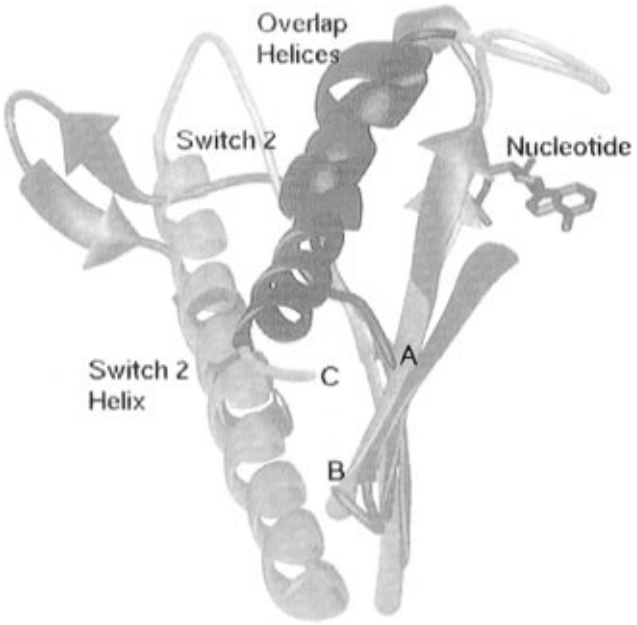


FIGURE 4: Ribbon diagram of the overlay of the crystallographic structures of ncd and chicken S1. The structures were aligned via a least-squares distance minimization of their respective P-loops and the flanking α-helices and $\beta$-strands. Only a portion of each molecule is shown in order to facilitate display of the similarities discussed in the text. Myosin is shown in yellow and ncd in cyan, except for the S1 sulfhydryl helix (dark blue) and the ncd α6-helix (red). The two helices clearly overlay each other. The ncd ligand (ADP) is in magenta. The helical domains following switch 2 are shown to also overlap. The following locations are additionally noted: A, C-terminus (Val-667) of the ncd crystal structure (our labeled Cys-670 is three residues away); B, N-terminus (Gly-347) of the ncd crystal structure; C, C-terminus of the myosin sulfhydryl helix (this connects to the myosin neck region).

α-helical region containing the widely studied reactive sulfhydryls, Cys-697 (SH-2) and Cys-707 (SH-1). To simplify terminology, we shall refer to this region as the "sulfhydryl helix". The sulfhydryl helix is adjacent to the very long α-helix which follows switch II in the lower 50K subdomain of S1. Crystallographic studies indicate that this latter, 50K subdomain, α-helix can be in different locations, depending upon the ligand at the nucleotide binding site, and that there is a concurrent angular shift in the sulfhydryl helix and the adjacent C-terminal end of the motor domain. Proper amplification of this motion via the helical lever may be sufficient to drive the power stroke (*4, 5, 23*).

The crystallographic structure of the ncd motor domain encompasses aa 346−667. Thus despite the fact that the labeled Cys-670 is not included in the crystallographic structure, the fact that it is only three residues beyond the end of the resolved crystal structure allows us to accurately locate its position. The final secondary structural element which is clearly delineated in the ncd crystal structure is the α6-helix shown as a ribbon diagram in the ncd structure (colored red; aa 654−664). As previously observed by Kull et al. (*1*), the α6-helix overlays the sulfhydryl helix in myosin when the structures are superimposed. The important observation is that our labeled Cys-670 is close by, only six residues beyond the α6-helix in the ncd structure. As the inter- and intramolecular forces defining a fixed crystal structure are clearly breaking down in the vicinity of our probe, we note that the secondary structure prediction protocols of both Chou and Fasman (*24*) and Garnier et al.

(*25*) indicate that the α6-helical domain could actually extend as far as aa 676, thus including our label site.

Our probe lies in a region of the ncd motor domain that contains the connection to the remainder (the other head and the rod portion) of the molecule. The connection between the motor domain and the rest of the molecule originates from the C-terminus in myosin and kinesin and from the N-terminus in ncd. Nonetheless, the structural elements that lead into the connections are adjacent to each other in the vicinity of both the myosin sulfhydryl helix and the ncd and kinesin α6-helices. They retain the same fundamental topology as shown in Figure 4. In myosin the sulfhydryl helix, or its cognate in kinesin, leads directly to the connection to the neck or stalk. In ncd, the polypeptide connecting the ncd motor domain to the backbone of the dimeric ncd form (entering the crystal structure at Arg-346) is close to the ncd α6-helix. All of these connections are topologically close to the conserved switch II helix that is likely to transmit conformational changes to this region. Arguments could be made that this is mere happenstance. Kull et al. (*1*), Sablin et al. (*2*), and Vale (*6*) detail additional, fundamental structural overlays that argue against this possibility and indeed lead to the hypothesis that myosin, ncd, and kinesin all derive from a common protein ancestor. Thus we appear to have labeled a region of very strongly conserved secondary structure across the family of actin-based and microtubule-based motor proteins.

*Protein Function.* In any biophysical or biochemical probe studies involving covalent modification of a protein, a crucial question concerns the effect of the modification on protein function. To address this concern, we have measured the effect of MSL labeling both on the affinity of ncd for microtubules in the presence of different ligands and on the ncd ATPase rate. As Table 1 shows, there is no significant change in any of these parameters when ncd and SL-ncd are compared. Furthermore, the ATPase rates and dissociation constants for ncd and SL-ncd given in Table 1 are comparable to those suggested by others (*14*) at the 140 mM ionic strength at which we worked. We do note, however, that we obtain a dissociation constant of SL-ncd·ADP·MT which is a factor of ∼2 higher than that obtained using unlabeled protein. Conversely, the factor of ∼2 is reversed in the presence of AMPPNP. There is likewise another factor of ∼2 difference in the ncd ATPase in the absence, but not presence, of microtubules. The important observation, however, is that, at worst, our covalent attachment of a spin probe to ncd Cys-670 results in only a very benign modification of protein function as monitored by either ATPase activity or microtubule binding.

With regard to the above, the important observation is that, for our probe at ncd Cys-670, current controversies concerning protein function following covalent modification are not an issue. This is distinctly different from the case for myosin, where labeling of a cysteine on the corresponding sulfhydryl helix of myosin is known to affect function in fibers (*13*) and in *in vitro* motility assays (*12*). Although the exact effect on the functionality of myosin is difficult to quantitate (e.g., see ref *26*), any decrease in function attests to the central role of this helix in the function of myosin. Mutation of a glycine in the center of the sulfhydryl helix abolishes the ability of myosin to function in the motility assays, again showing the importance of the structural integrity of this helix (*27*). Our results suggest that the introduction of a cysteine into myosin a few amino acids toward the C-terminus from the sulfhydryl helix, via mutagenesis, could yield an exceptionally useful construct, while having the potential for avoiding the above mentioned, down-regulation of function occurring when the myosin sulfhydryl helix itself is covalently modified.

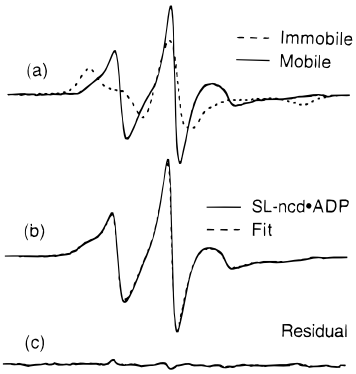


FIGURE 5: (a) Mobile (solid line) and immobile (dashed line) deconvolution spectra for SL-ncd with ADP as the nucleotide. For better visualization, the immobile spectrum is normalized to represent twice as many spins as the mobile spectrum. (b) Spectrum of 50 $\mu$M SL-ncd in solution with 2 mM ADP (solid line) and the least-squares fit of this spectrum (dashed line) using the mobile and immobile deconvolution spectra (Figure 3a). The best fit was with 32% of the spectral intensity coming from the immobile component. (c) Difference spectrum between the solid and dashed fits of (b) indicating the quality of the fit.

*Immobile and Mobile Components of the EPR Spectra.* The obvious shift in spectral intensity from peak $P_2$ to peak $P_1$ when SL-ncd binds to microtubules indicates a shift between two populations of probes. In the absence of microtubules, a population of probes that are highly mobile with respect to the protein, dominates the spectra. In the presence of microtubules, the probes become much more immobilized. In order to assess better the properties of these two populations, the two components were deconvoluted by subtracting a spectrum that had a high fraction of the mobile component, SL-ncd·ADP, from one that had a high fraction of the immobile component, a SL-ncd·ADP·MT pellet. One is able to subtract the mobile component with high precision because it contributes intensity at the peak $P_2$, and it is solely responsible for the sharp shoulder of intensity just upfield from the central peak. The combination of spectral components which minimized the intensity due to $P_2$ was taken as representing the spectrum of probes immobilized with respect to the protein. Once the immobilized component was obtained, it could then be subtracted from an observed spectrum to obtain the mobile component. The results are shown in Figure 5a. The solid line and the dashed line are the spectral components representing the mobile and the more immobilized probes, respectively. In order to better display the immobile spectral component, it has been normalized to represent twice the molar quantity of spins as the mobile spectral component. Similar protocols yielded immobilized and mobile spectra when AMPPNP was the ligand as shown in Figure 6a, similarly normalized. No spectrum of a pellet with microtubules was possible with ATP. The deconvolution spectra (not shown) were instead obtained from the spectra of SL-ncd, ATP, and microtubules in solution as in Figure 2f.

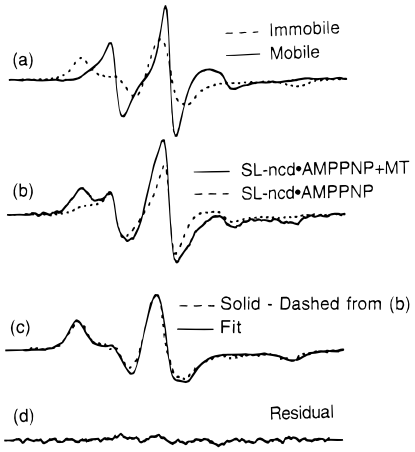


FIGURE 6: (a) Mobile (solid line) and immobile (dashed line) deconvolution spectra for SL-ncd with AMPPNP as the nucleotide. (b) The solid line is the spectrum obtained from an experiment containing 50 $\mu$M SL-ncd, 50 $\mu$M microtubules, and 2 mM AMPPNP. The dashed line is the spectrum obtained from 50 $\mu$M SL-ncd and 2 mM AMPPNP in solution in the absence of microtubules but normalized to represent the unbound, 17 $\mu$M SL-ncd•AMPPNP predicted from the dissociation constant to be present in the solid-line spectrum. (c) The dashed line is the spectrum obtained when the unbound SL-ncd in (b) (dashed line) is subtracted from the spectrum obtained in the presence of microtubules (b, solid line). The solid line is a least-squares fit of this spectrum as a sum of the deconvolution spectra in (a). (d) The difference spectrum between the solid and dashed lines in (c).

There is no statistically significant difference in the spectra of the mobile component obtained in the presence of either ADP, ATP, or AMPPNP. The spectral shape of the mobile component suggests that it arises from probes which are free to undergo almost isotropic, Brownian rotations, with a rotational correlation time of 2−4 ns. The small low-field shoulder in the mobile spectral component, however, shows that this component is complex, containing a small fraction that has a slower mobility.

The immobilized spectral components obtained in the presence of microtubules were likewise virtually identical for bound ADP, AMPPNP, or ATP. Averaging over all deconvolutions, the low-field to high-field splitting between the immobilized components, $P_1$ and $P_3$, was 6.32 ± 0.03 mT (11 observations). Modeling studies have shown that the splitting between $P_1$ and $P_3$ is a measure of the degree to which the probe is immobilized with respect to the protein (*28*). In the rigid limit, when the probe is completely immobilized with respect to the protein, the $P_1$ to $P_3$ splitting of MSL was 7.2 mT. The observed 6.3 mT splitting is representative of an EPR probe which is covalently attached to the protein and constrained to move within a cone with a half-angle of ∼29°, independent of nucleotide. When compared to the immobile component spectra of AMPPNP and ATP, we did note that there was a slightly broader upfield shoulder at $P_2$ in the presence of ADP. Although this component was reproducible (four observations), it represented <4% of the total spins, and thus any nucleotide-induced differences were very small.

Is there an immobile component of the spectrum of SL-ncd•nucleotide in the absence of microtubules? The spectrum of SL-ncd•ADP contained a low-field shoulder suggesting the potential presence of an immobilized component. To estimate this immobilized fraction, the spectrum of SL-ncd•ADP (solid line, Figure 5b) was fit using a least-squares minimization as the sum of the mobile and the immobile spectral components obtained in the presence of ADP (Figure 5a). The minimized fit (dashed line, Figure 5b) implied that 32% of the spectral intensity was provided by the immobile spectral component. Figure 5c shows the difference spectrum between the dashed and solid lines in Figure 5b, indicating the goodness of fit. Averaging over all such least-squares fits, the immobile component of the spectrum of SL-ncd•ADP in solution represented 34 ± 3% (10 observations) of the total spins. Thus at room temperature, about one-third of the probes were immobilized with respect to the protein in the absence of microtubules; about two-thirds were mobile. Similar low-field shoulders were observed with AMPPNP or ATP as the ligand. For AMPPNP, least-squares fits to the spectra of SL-ncd•AMPPNP in solution using the mobile and immobile AMPPNP deconvolution spectra (Figure 6a,b) gave an immobile component of 36 ± 4% (seven observations) of the total spin. With ATP as the nucleotide, a comparable immobile component of 35 ± 2% (seven observations) was obtained.

Is there a mobile component of the spectrum of bound, ncd•ligand•MT? We have shown that, for SL-ncd in solution, the protein is in two conformations, one in which the spin-label is highly mobile with respect to the protein and one in which the probe is more immobilized with respect to the protein. In the presence of microtubules, a fraction of the residual mobile component remains. Is this simply the result of the equilibrium between SL-ncd bound to microtubules and SL-ncd free in solution? To address this question, the following protocol was used as shown in Figure 6 with AMPPNP as ligand. For given initial concentrations of SL-ncd and microtubules, the concentrations of SL-ncd•AMPPNP and SL-ncd•AMPPNP•MT could be determined from the measured dissociation constant (Table 1). The EPR spectrum of a known concentration of SL-ncd•AMPPNP in solution was multiplicatively scaled to correspond to this concentration. It was then subtracted from the spectrum of a mixture of SL-ncd•AMPPNP and SL-ncd•AMPPNP•MT in solution. This is shown in Figure 6b. The solid line is the EPR spectrum resulting from a buffer containing 50 $\mu$M SL-ncd and 50 $\mu$M MT. The dissociation constant implied that 17 $\mu$M SL-ncd•AMPPNP remained in solution at equilibrium. The dashed line in Figure 6b is a spectrum obtained from 50 $\mu$M SL-ncd•AMPPNP in solution, multiplicatively scaled to 17 $\mu$M. The dashed line in Figure 6c is the spectrum obtained by subtracting the dashed spectrum from the solid line spectrum in Figure 6b. This difference spectrum was taken to represent the spectrum of SL-ncd•AMPPNP•MT and subtracted from the spectrum in Figure 2d. This residual spectrum (Figure 6c) was thus taken to represent the spectrum of SL-ncd•AMPPNP•MT and was then fit as a least-squares minimization sum of the mobile and immobile deconvolution spectra (Figure 6a). The least-squares fit is shown as the solid line in Figure 6c. Figure 6d is the difference spectrum from Figure 6c, showing the quality of the fit. The fitted spectrum contained a mobile component of 2.2%. Averaging over all such fits, we found a mobile component in the spectrum of bound SL-ncd•AMPPNP•MT of 3.3 ± 4.1% (six observations). With ADP as the nucleotide, and using the deconvoluted spectra of Figure 4a, the corresponding mobile component was 1.5 ± 4.0% (six observations); with ATP, the mobile component was 4.0 ± 6.2% (four observations). Thus although we

cannot conclusively rule out the presence of a mobile component in the spectrum of SL-ncd bound to microtubules, any such fraction is going to be rather small.

The rotational correlation time of ncd, ~30 ns, is relatively rigid on the EPR time scale. It is much slower than that of the mobile component, 2−3 ns. Thus the decreased mobility of the probe upon the binding of ncd to microtubules does not arise simply from the slower tumbling rate of microtubule-bound SL-ncd.

*Effect of Temperature.* Our probe at Cys-670 has identified two states of ncd which give rise to different spectral components. These two spectral components could arise from a minor shift in the position of a single side chain, or they could reflect a major shift in the conformation of a substantial region of the protein. To address this question, we have investigated the relative immobile and mobile fractions in the spectra of SL-ncd as a function of temperature in order to better define the thermodynamics associated with this transition. Figure 3a showed an immobile-to-mobile shift as temperature increased for SL-ncd·ADP in solution. More extensive data as a function of temperature are given in Figure 3b (solid points; right vertical axis). The magnitudes of the immobilized fractions were determined from the previously described spectral components as in Figure 5a. Letting $K$ = [immobile fraction]/[mobile fraction] be the equilibrium constant between the two states, Figure 3b gives $-R \ln(K)$ for the titration data (open circles; left vertical axis). Using the van't Hoff equation, a least-squares linear fit ($r = 0.98$) to the data yields a mean value for $\Delta H° = -75.3$ kJ/mol. The data are significantly better fit by a parabola ($r = 0.999$) with the slope giving values for $\Delta H°$ which varied from −40 kJ/mol at 2 °C to −105 kJ/mol at 25 °C. Less extensive spectra taken with AMPPNP and ATP as ligands (triangles and squares, Figure 3b) indicate that the temperature dependence is not altered by the nature of the bound ligand.

Changes in enthalpy and entropy of the above magnitude indicate that we are dealing with a rather large structural and energetic change within the protein. The enthalpy change associated with the binding of a small molecule like the spin probe to the protein surface would be expected to be a small fraction (only a few kilojoules per mole) of the enthalpy change we observed. To put our observed value of −75 kJ/mol in better perspective, we note that the change in enthalpy associated with ATP hydrolysis by myosin is approximately −50 kJ/mol (*29*). The change in enthalpy for the unfolding of a small protein (100−150 aa) is approximately 300 kJ/mol, and thus our observed enthalpy change would correspond to the unfolding of 20−30 residues (*30*). Similar observations of two distinct states of myosin with large enthalpy and entropy differences have previously been reported by Shriver and Sykes (*31, 32*) and by Cheung and co-workers (*33, 34*). These observations, along with the present results, suggest that motor proteins exist in two conformations with approximately equal free energies, but with different enthalpies and entropies. The binding of polymers can alter the relative proportions of these two populations.

*Implications of the Spectra for Protein Mechanics.* One possibility for our observation of a mobile-to-immobile transition upon the binding of SL-ncd to microtubules is that Cys-670 is part of the microtubule binding site. The spin probe would then trivially become immobilized as it is simply sandwiched between SL-ncd and the microtubule upon formation of the SL-ncd·ligand·MT complex. Recent electron cryomicroscopy based three-dimensional reconstructions of both dimeric ncd and dimeric kinesin bound to microtubules (*35*) allow one to define the site for microtubule binding approximately and argue against the possibility that our probe is at the microtubule binding site. The three-dimensional reconstructions of ncd show the motor domains to be joined at one end, with the microtubule binding site located toward the other end of the single attached ncd head. Taking the joined domain between the heads to be close to the commonly shared region where the necks enter the motor domains and observing from the crystal structures that this entry point is very close to our labeled Cys-670, our spin-label is closer to the motor head−motor head junction than to the microtubule binding site.

Analysis of the $P_1$ to $P_3$ splitting for the spectra of SL-ncd·ligand free in solution provides additional support for our conclusion that the immobilized state observed in the presence of microtubules is the same immobilized state observed in the spectra of SL-ncd free in solution and not an immobilized state produced by sandwiching the spin probe between ncd and the microtubule upon binding. Subtracting the mobile components (Figures 5a and 6a) from the spectra of SL-ncd·ADP or SL-ncd·AMPPNP, as in Figures 5 and 6, yielded spectra of the immobile component with a $P_1$ to $P_3$ splitting of 6.28 ± 0.06 mT (10 observations). Alternatively, as the experimental temperature was lowered in the absence of microtubules, the immobile component of the spectra of SL-ncd·ADP and SL-ncd·AMPPNP increased significantly. A similar deconvolution of spectra taken at 2 and 5 °C yielded a value for the $P_1$ to $P_3$ splitting of 6.24 ± 0.03 mT (10 observations). These values for the splitting are virtually identical to the 6.3 mT value previously noted for the splitting of the immobile spectral component. If the immobilization were the result of trivially restricting the motion of the probe between ncd and the microtubule, one would instead expect the splitting to change as the half-angle of the cone in which the probe was located changed as the microtubule restricted the motion of the probe. Thus the simplest interpretation of our spectra is that there is a direct path of communication between the motor domain−microtubule interface and the region where the motor domain joins the neck.

A similar communication is seen between the motor−actin interface and the homologous helix in myosin. The binding of actin modifies the reactivities of SH-1 and SH-2 (*36, 37*) and alters the mobility of probes attached to SH-1 or SH-2 (*38−40*). Thus, although the actin-induced changes in probe spectra are not as dramatic as seen here, there is clear evidence that actin does perturb the conformation of this region.

The presence of a direct route of communication between the motor−polymer interface and the region that we have labeled may have important implications for models of motor protein function. The energetics of the actomyosin interaction show that the power stroke occurs in the cycle coincident with the formation of a stronger bond between actin and myosin and that the free energy released by the formation of the stronger bond is used to drive the power stroke [reviewed by Cooke (*41*)]. Thus our probe appears to monitor a conformational change in the motor−neck region, driven by formation of the motor−polymer interface which

may be the conformational change that drives force generation. A similar route of communication occurs for both myosin and ncd.

In summary, we have placed an EPR probe on Cys-670 of ncd. The probe does not affect protein function as monitored by microtubule binding or ATPase. The probe appears to detect a conformational change close to the head−neck junction which occurs when the microtubule binds at a distant location to initiate the working power stroke. Although previous studies with myosin have suggested that formation of a strong actomyosin bond induces conformational changes near the motor domain−neck junction, our probe at Cys-670 of ncd provides a significantly less ambiguous reporter signal of such a conformational change. This further suggests that fundamental homologies in the chemomechanical transduction step may exist between microtubule-based and actin-based motor proteins.

This is the first successful application of EPR spectroscopy to monitor conformational changes in a microtubule-based motor protein. Cys-670 may prove to be a useful site for further probe studies. Such studies are now in progress.

## ACKNOWLEDGMENT

We thank Jamil Kananni and the UCSF peptide sequencing facility for assistance in the ncd peptide sequencing studies and A. Ruby for providing copious quantities of bacterial-expressed ncd. We extend special thanks to E. Sablin and J. Kull for providing the X-ray crystallographic coordinates of ncd and kinesin prior to publication and for their assistance in protein purification.

## REFERENCES

1. Kull, F. J., Sablin, E. P., Lau, R., Fletterick, R. J., and Vale, R. D. (1996) *Nature 380*, 550−555.
2. Sablin, E. P., Kull, F. J., Cooke, R., Vale, R. D., and Fletterick, R. J. (1996) *Nature 380*, 555−559.
3. Rayment, I., Rypniewski, W. R., Schmidt-Base, K., Smith, R., Tomchick, D. R., Benning, M. M., Winkelmann, D. A., Wesenberg, G., and Holden, H. M. (1993) *Science 261*, 50−57.
4. Fischer, A. J., Smith, C. A., Thoden, J., Smith, R., Sutoh, K., Holden, H. M., and Rayment, I. (1995) *Biochemistry 34*, 8960−8972.
5. Smith, C. A., and Rayment, I. (1996) *Biochemistry 35*, 5404−5417.
6. Vale, R. D. (1996) *J. Cell Biol. 135*, 291−302.
7. Cooke, R., Crowder, M. S., and Thomas, D. D. (1982) *Nature 30*, 778−778.
8. Fajer, P. G., Fajer, E. A., Brunsvold, N. J., and Thomas, D. D. (1988) *Biophys. J. 53*, 513−524.
9. Thomas, D. D., and Cooke, R. (1980) *Biophys. J. 32*, 891−905.
10. Crowder, M. S., and Cooke, R. (1987) *Biophys. J. 51*, 323−333.
11. Alessi, D. R., Corrie, J. E. T., Fajer, P. G., Ferenczi, M. A., Thomas, D. D., Trayer, I. P., and Trentham, D. R. (1992) *Biochemistry 31*, 8043−8054.
12. Root, D. D., and Reisler, E. (1992) *Biophys. J. 63*, 730−740.
13. Bell, M. G., Matta, J. J., Thomas, D. D., and Goldman, Y. E. (1995) *Biophys. J. 68*, 360s.
14. Shimizu, T., Sablin, E., Vale, R. D., Fletterick, R., Pechatnikova, E., and Taylor, E. W. (1995) *Biochemistry 34*, 13259−13266.
15. Bradford, M. M. (1976) *Anal. Biochem. 72*, 248−254.
16. Murphy, D. B., and Borisy, G. G. (1975) *Proc. Natl. Acad. Sci. U.S.A. 72*, 2696−2700.
17. Ma, Y.-Z., and Taylor, E. W. (1995) *Biochemistry 34*, 13242−13251.
18. Pate, E., Franks, K., White, H. D., and Cooke, R. (1993) *J. Biol. Chem. 268*, 10046−10053.
19. Huang, T.-G., and Hackney, D. D. (1994) *J. Biol. Chem. 269*, 16508−16511.
20. Kanaani, J., Maltby, D., Focia, P., and Wang, C. C. (1995) *Biochemistry 34*, 14987−14996.
21. Kodama, T., Fukui, K., and Kometani, K. (1986) *J. Biochem. 99*, 1465−1472.
22. Walker, J. E., Saraste, M., Runswick, M. J., and Gay, N. J. (1982) *EMBO J. 1*, 945−951.
23. Holmes, K. C. (1996) *Curr. Opin. Struct. Biol. 6*, 781−789.
24. Chou, P. Y., and Fasman, G. D. (1978) *Adv. Enzymol. 47*, 45−147.
25. Garnier, J., Osguthorpe, D. J., and Robson, B. (1978) *J. Mol. Biol. 120*, 97−120.
26. Crowder, M. S., and Cooke, R. (1984) *J. Muscle Res. Cell Motil. 5*, 131−146.
27. Kinose, F., Wang, S. X., Kidambi, Moncman, C. L., and Winkelman, D. A. (1996) *J. Cell Biol. 134*, 895−909.
28. Griffith, O. H., and Host, P. C. (1976) in *Spin Labeling: Theory and Applications*, (Berliner, L. J., Ed.) Academic Press, New York.
29. Curtin, N. C., and Woledge, R. C. (1979) *J. Physiol. 288*, 353−366.
30. Creighton, T. E. (1993) *Proteins: Structures and Molecular Properties*, p 311, W. H. Freeman and Co., New York.
31. Shriver, J. W., and Sykes, B. D. (1981) *Biochemistry 20*, 6357−6362.
32. Shriver, J. W., and Sykes, B. D. (1982) *Biochemistry 21*, 3022−3028.
33. Aguirre, R., Lin, S.-H., Gonsoulin, F., Wang, C.-K., and Cheung, H. C. (1989) *Biochemistry 28*, 799−807.
34. Lin, S.-H., and Cheung, H. C. (1991) *Biochemistry 30*, 4317−4322.
35. Arnal, I., Metoz, F., DeBonis, S., and Wade, R. H. (1996) *Curr. Biol. 6*, 1265−1270.
36. Duke, J., Takashi, R., Ue, K., and Morales, M. F. (1976) *Proc. Natl. Acad. Sci. U.S.A. 73*, 302−306.
37. Zhao, L., Naber, N., and Cooke, R. (1995) *Biophys. J. 68*, 1980−1990.
38. Thomas, D. D., Seidel, J. C., Gergley, J., and Hyde, J. S. (1975) *J. Supramol. Struct. 3*, 376−390.
39. Burghardt, T. P., and Ajtai, K. (1985) *Proc. Natl. Acad. Sci. U.S.A. 82*, 8478−8482.
40. Burghardt, T. P., and Ajtai, K. (1986) *Biochemistry 25*, 3469−3478.
41. Cooke, R. (1997) *Physiol. Rev.* (in press).

BI9706881